Chinese Chemical Letters 33 (2022) 308–313

Contents lists available at ScienceDirect

Chinese Chemical Letters

journal homepage: www.elsevier.com/locate/cclet

Green rapid synthesis of Cu_2O/Ag heterojunctions exerting synergistic antibiosis

Feiyue Hu[a], Bo Song[a], Xiaohan Wang[a], Shen Bao[a], Siyang Shang[a], Shupei Lv[a], Bingbing Fan[a,*], Rui Zhang[a,c], Jingguo Li[a,b,*]

[a] School of Materials Science and Engineering, Zhengzhou University, Zhengzhou 450001, China
[b] People's Hospital of Zhengzhou University, Henan Provincial People's Hospital, Zhengzhou 450003, China
[c] School of Material Science and Engineering, Luoyang Institute of Science and Technology, Luoyang 471023, China

ARTICLE INFO

Article history:
Received 30 April 2021
Revised 5 July 2021
Accepted 7 July 2021
Available online 13 July 2021

Keywords:
Cu_2O/Ag heterojunctions
Green synthesis
Microwave-assisted
Antibacterial
Synergistic effect

ABSTRACT

Semiconductor-noble metal composite has become a research focus due to its superior performance compared with its respective component. Although various methods have been developed to synthesize semiconductor-noble metal heterostructures, most of them are relatively complex multistep and use toxic reactants of high cost and risk. In this work, a series of Cu_2O/Ag heterojunctions were quickly prepared in one step *via* simple microwave-assisted green route. XRD, SEM, TEM, EDS, XPS, *etc*. were used to characterize obtained products, and the results indicate a Cu_2O/Ag metal-semiconductor heterojunction in micro-nano size was fabricated successfully. In addition, antibacterial behavior of Cu_2O/Ag heterojunctions against *E. coli* and *S. aureus* were investigated. Owing to the synergistic effect of Cu_2O and Ag, the heterojunction exhibits much better antibacterial performance than the pristine Cu_2O does. This work provides new insights into the green design and fabrication of surface-modified Cu_2O hybrid multifunctional materials for antibacterial applications.

Semiconductor-noble metal composites of hybrid nanostructure could retain original merits of each constituent and simultaneously display attractive comprehensive properties [1,2]. Various methods have been developed to synthesize semiconductor-noble metal heterostructures by assembling noble metal nanoparticles such as Ag, Au, Pd, and Pt to the surface of semiconductor [3,4].

In recent years, some scholars have proposed to construct a metal-semiconductor heterojunction to promote the transfer of electrons and holes between Cu_2O and Ag, and further improved the stability and property of Cu_2O [5]. As an important semiconductor of direct band-gap of about 2.1 eV, non-toxicity, low price, and good environmental friendliness [6,7], Cu_2O has aroused much interest owing to its potential applications, especially in antimicrobial area. Meanwhile, Ag is a relatively cheap precious metal of excellent broad-spectrum, strong durability and safety, and has showed usability in various medical areas [8,9]. Microbes hazard real world seriously, such as health and safety issues of human beings, metal surface corrosion and equipment-related infections [10–13]. Yet, only a few researches focused on the antibacterial properties of Cu_2O/Ag heterojunctions [14], and others mostly investigated their photocatalytic applications and surface-enhanced Raman scattering (SERS) [15-17]. Most semiconductor-noble metal composites are prepared using relatively complex multistep methods and toxic reactants, which has the characteristics of high energy consumption and risk. Therefore, it is quite necessary to explore the green rapid synthesis of Cu_2O/Ag as an emerging efficient fungicide in the field of pollution-free sterilization.

In this communication, a simple microwave-assisted method was used to prepare Cu_2O/Ag heterojunction and the antibacterial behavior of it was investigated. By bringing advantages of microwave synthesis such as energy-saving and large efficiency, Cu_2O/Ag heterojunctions in micro-nano size could be produced in just a few minutes. Meanwhile, this method is green and environmentally friendly by using glucose as reducing agent and safe and reliable without using strong alkali.

Experimental details are provided in Supporting information. As-prepared Cu_2O/Ag hybrids of various molar ratios of $AgNO_3$:$Cu(Ac)_2$ (0, 1:15, 1:9 and 1:3, respectively) are indexed as T1, T2, T3 and T4. Fig. 1A exhibits the simple microwave-assisted one-step synthesis of Cu_2O/Ag heterojunctions. Fig. 1B shows the morphology of as-prepared composites and it can be easily found that the size of Cu_2O particles decreased obviously with the in-

* Corresponding authors.
E-mail addresses: fanbingbing@zzu.edu.cn (B. Fan), lijingguo@zzu.edu.cn (J. Li).

https://doi.org/10.1016/j.cclet.2021.07.018
1001-8417/

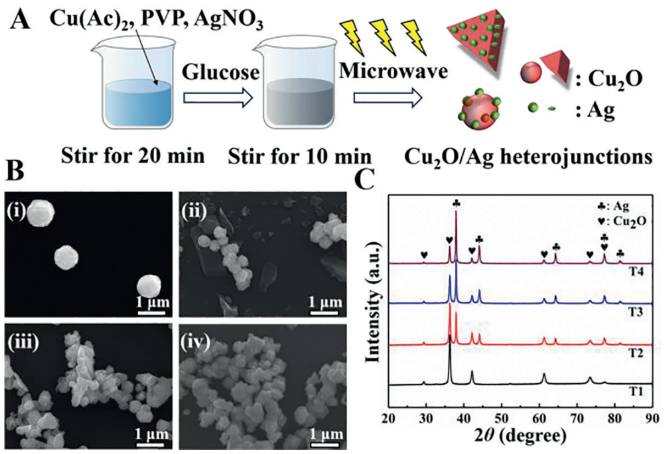

Fig. 1. (A) Schematic illustration of the facile method to prepare samples. (B) SEM images of prepared Cu_2O/Ag composites: (i) T1, (ii) T2, (iii) T3 and (iv) T4. Scale bar: 1 μm. (C) XRD patterns of prepared Cu_2O/Ag composites. For interpretation of the references to color in this figure legend, the reader is referred to the web version of this article.

crease of molar ratio of $AgNO_3$:$Cu(Ac)_2$ (n_{AgNO3}:$n_{Cu(Ac)2}$). The average particle size of pure Cu_2O prepared without addition of $AgNO_3$ (T1) is between 0.9 μm and 1.2 μm (Fig. 1B, image i). When n_{AgNO3}:$n_{Cu(Ac)2}$ = 1:15, Cu_2O particles of the composites become much smaller (400-500 nm) and Ag particles in flake geometry exist alone (Fig. 1B, image ii). When n_{AgNO3}:$n_{Cu(Ac)2}$ increases to 1:9, a triangular sheet-like heterostructure of a side length of about 700 nm appears (Fig. 1B, image iii). The formation mechanism of triangular flakes could be in following routine: Silver nanosheets generates initially, and then act as the nucleating substrate of Cu_2O; Cu_2O finally develops into a triangular flake heterojunction structure in the microwave-assisted synthesis process. Therefore, Cu_2O particles and Ag would form close contact in this step. In the same way, a lot of Ag nanoparticles generate and act as nucleation sites before Cu_2O begins to nucleate, which brings about the decrease in size of Cu_2O. When of n_{AgNO3}:$n_{Cu(Ac)2}$ goes up further, Ag/Cu_2O triangular flakes disappear and the particles tend to agglomerate (Fig. 1B, image iv).

Fig. 1C shows the XRD patterns of prepared samples. It could be easily found that all the composites show strong diffraction peak intensity at the characteristic peak locations corresponding the Cu_2O phase of cubic crystal structure (space group: Pn3m, JCPDS 5-667) with fitted lattice parameter of a = 0.430 nm. In addition, there are extra peaks (plum notations) emerging in the XRD patterns of Ag/Cu_2O products (T2, T3, T4) due to the introduction of Ag, and the XRD peaks at 2θ degrees of 38.116°, 44.277°, 64.426°, 77.472°, and 81.536° can be attributed to the (111), (200), (220), (311), and (222) crystalline planes of the FCC crystalline structure of Ag, respectively (space group: Fm-3m, JCPDS 4-783) with fitted lattice parameter of a = 0.409 nm [18]. Meanwhile, no other peaks representing impurity are identified in XRD patterns, indicating that the high purity of the as-obtained products. With the increase of n_{AgNO3}:$n_{Cu(Ac)2}$, the intensity of the Ag peaks increased obviously, which indicated that the Ag content in the composites was positively correlated with the amount of $AgNO_3$ added.

Morphology and microstructure of T3 were further characterized by TEM and HRTEM and shown in Fig. 2A. Image i in Fig. 2A demonstrates the unique geometry of triangular and spherical heterostructures of T3, which is consistent with the geometry observed using SEM (Fig. 1B, image iii). Image ii in Fig. 2A indicates an obvious interface between Ag and Cu_2O at larger magnification and it can be seen clearly from the TEM image that the thickness of Ag layer is around 30 nm. The interplanar spacing shown in the left area of image iii in Fig. 2A is 0.245 nm, which corresponds to the spacing between the (111) lattice planes of Ag. While the interplanar spacing in the right area is 0.298 nm, corresponding to the spacing between the (110) lattice planes of Cu_2O. Image iv in Fig. 2A is the selected-area electron diffraction (SAED) image of the interface between Ag and Cu_2O, indicating that the composite has a single-crystal structure. It is clear that the generation of Cu_2O/Ag heterojunction occurs during the microwave synthesis process according to the above results.

EDS mapping of T3 is conducted and the result is shown in Fig. 2B. It confirms the coexistence of Ag, Cu, and O elements in the Cu_2O/Ag heterojunctions and further proves that the composite material is not just a simple mixture of Ag particles and Cu_2O particles, but a micro-nano composite that is tightly bound together. UV-visible absorption spectra of prepared composites are shown in Fig. 2C. It can be seen that Cu_2O has a good absorption in the range of 400-600 nm. The absorption of the Cu_2O/Ag heterojunctions in the visible light range is significantly enhanced after comparing curves T2, T3 and T4 with T1. The band gap can be determined from the tangent intercept of the $(\alpha h\nu)^2$ ~ $(h\nu)$ graph, where α is the absorption coefficient, h is the Planck constant, and ν is the frequency (Fig. 2D). The band gap energies of the original Cu_2O microspheres and the Cu_2O/Ag heterojunction obtained by adding silver nitrate gradually are ~2.1, 1.9, 1.6, and 1.4 eV, respectively. As the Ag content increases, the band gap energy decreases. The red shift of the adsorption edge and the reduction of band gap energy are mainly attributed to the Schottky effects between Ag and Cu_2O [19].

XPS scan is performed to further investigate the composition and the elemental states of T3. The binding energies in the XPS spectra presented in Figs. 2E-H are calibrated by referring that of C 1s (284.8 eV). In Fig. 2E, all peaks in the curve can be ascribed to Cu, Ag, O and C elements. The presence of C mainly comes from the hydrocarbon of the XPS instrument itself. The peaks at 932.1 and 952.1 eV are assigned to the Cu $2p_{3/2}$ and Cu $2p_{1/2}$ of Cu_2O (Fig. 2F). No peak corresponding to CuO (933.6 eV) is detected. The peaks at 368.2 and 374.2 eV should be assigned to Ag $3d_{5/2}$ and Ag $3d_{3/2}$, respectively (Fig. 2G), and the splitting of the 3d doublet is 6.0 eV, which hints that Ag is of metallic nature [18]. The O 1s region shown in Fig. 2H could be fit into two peaks. The main peak (530.7 eV) is attributed to Cu-O in Cu_2O whereas the minor peak (531.9 eV) can be ascribed to O adsorbed at the surface of the sample [20].

Minimal inhibition concentration (MIC) and minimal bactericidal concentration (MBC) can be used to quantitatively evaluate the antibacterial property of substrates. The microplate reader is a routine instrument for enzyme-linked immunosorbent assay, which utilizes material absorption spectroscopy and visible light colorimetric technique. It is widely used in microbiology because of its rapid detection and tracing of microbe microstructures. Due to the scattering and absorption of bacteria, when light passes through the bacterial suspension, the optical density (OD) value can represent the concentration of bacteria within a certain range [21]. The larger the OD value, the higher the bacterial content, and the poorer the antibacterial performance. Therefore, the antibacterial effect of antimicrobial agents can be characterized by measuring the OD of the bacterial solution with a spectrophotometer.

MICs of Cu_2O/Ag heterojunctions against Gram-negative bacteria (*E. coli*) and Gram-positive bacteria (*S. aureus*) were determined by Methyl Thiazolyl Tetrazolium (MTT) assay. As shown in Figs. 3B and D, at higher Cu_2O/Ag concentration, the cell viability is lower than that at other small concentrations of Cu_2O/Ag. This is due to that high concentration Cu_2O/Ag heterojunctions could directly inhibit the growth of bacteria. When the inorganic antibiotics are of small concentrations, bacteria propagate fast since they show large bacterial cell viability.

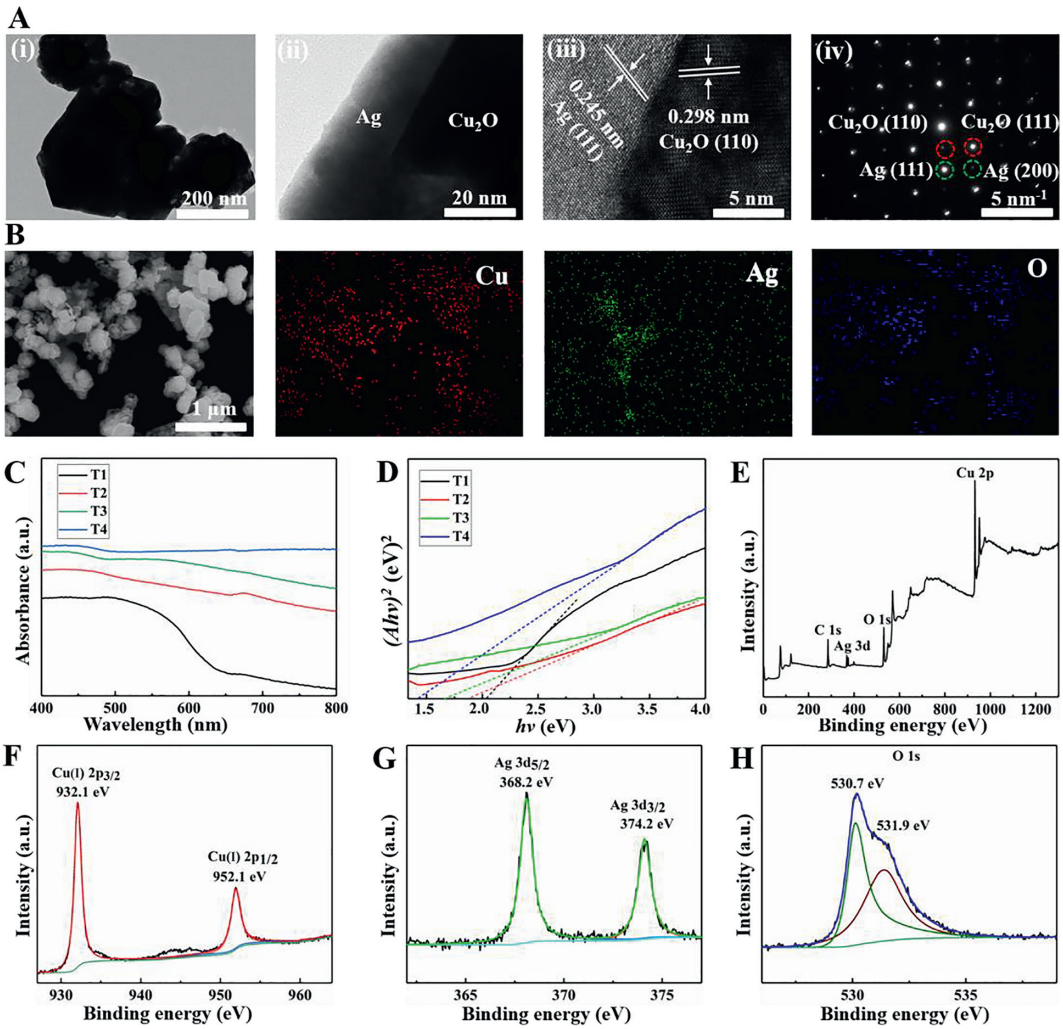

Fig. 2. (A) Morphology and composition of Cu_2O/Ag heterostructure in sample T3: (i) Cu_2O/Ag heterostructure morphology; (ii) edge of heterostructure in (i) at larger magnification; (iii) HRTEM image of heterostructure showing composition information, and (iv) SAED pattern of (iii). (B) Elemental mappings of T3. (C) UV-visible absorption spectra of Cu_2O/Ag composites. (D) Plots of $(\alpha h\nu)^2$ *vs.* $h\nu$ for the Cu_2O/Ag composites. (E) XPS full spectrum of the sample T3. (F) Cu 2p spectrum. (G) Ag 3d spectrum. (H) O 1s spectrum.

To quantitatively assess the antibacterial activities of Cu_2O/Ag heterojunctions, MICs and MBCs of *E. coli* and *S. aureus* bacteria are shown in Table S1 (Supporting information). MICs of T1 (pure Cu_2O) against *E. coli* and *S. aureus* are 7.8 and 15.6 μg/mL, respectively. When the Cu_2O/Ag heterojunction is introduced, MICs of both bacteria decrease dramatically. MICs in T3 trail against *E. coli* and *S. aureus* are 0.5 and 1.0 μg/mL, presenting a best antibacterial performance in this work. This superiority is attributed to the unique triangular sheet heterostructure of Cu_2O/Ag, which provides a stronger synergistic effect on the antibacterial activity when compared with single Cu_2O or Cu_2O/Ag heterojunctions of other ratios. In addition, compared with other antimicrobial agents, such as Cu_2O [22], Cu_2O@ZrP [23] and RGO-Cu_2O [24], our Cu_2O/Ag heterojunctions are equally excellent or even more outstanding in antimicrobial applications. Then, to further evaluate the antimicrobial activity of the materials, MBC tests against *E. coli* and *S. aureus* were performed in all sample trails and by using colony counting methods (Figs. 3A and C). Obviously, *E. coli* and *S. aureus* Colony Forming Units (CFUs) sharply decrease with increasing concentrations of antibacterial agents. All samples including T1 show a bactericidal effect on both two kinds of bacteria and T2, T3 and T4 are more potent than T1. Like the results of MTT assay mentioned above, T3 has the highest antibacterial performance among all four samples. Another point needs to be emphasized is, all four samples show a better antibacterial effect when dealing with *E. coli* is. This is due to the peptidoglycan layer of *E. coli* is thicker than that of *S. aureus*, making *S. aureus* less sensitive to nanoparticles than *E. coli* [25].

In order to study the antibacterial mechanism of Cu_2O/Ag heterojunctions, two fluorescent nucleic acid dyes, 4′,6-diamidino-2-phenylindole (DAPI) and polyimide (PI), were used to stain bacteria. DAPI marks both live and dead cells, while PI can only penetrate cells having compromised or damaged membranes (dead cells). Therefore, they can be used to test whether the bacteria are live (blue) or dead (red). As shown in Fig. 4A, *E. coli* and *S. aureus* cells are almost completely stained by PI, which indicates damaged cell walls and membranes and/or mass cell death after treatment using 50 μg/mL T3 solution for 1 h [26].

Zeta potential measurement was made on all the samples (Table S2 in Supporting information). The zeta potential of single Cu_2O was −2.6 mV. While the zeta potential of all Cu_2O/Ag heterojunctions was greater than 10 mV, which can greatly improve the adsorption contact between the samples and the bacteria because the surface of the bacteria is generally negatively charged [27]. T3 composites have the best adsorption capacity for bacteria, which may bring mechanical damage to the bacterial cell mem-

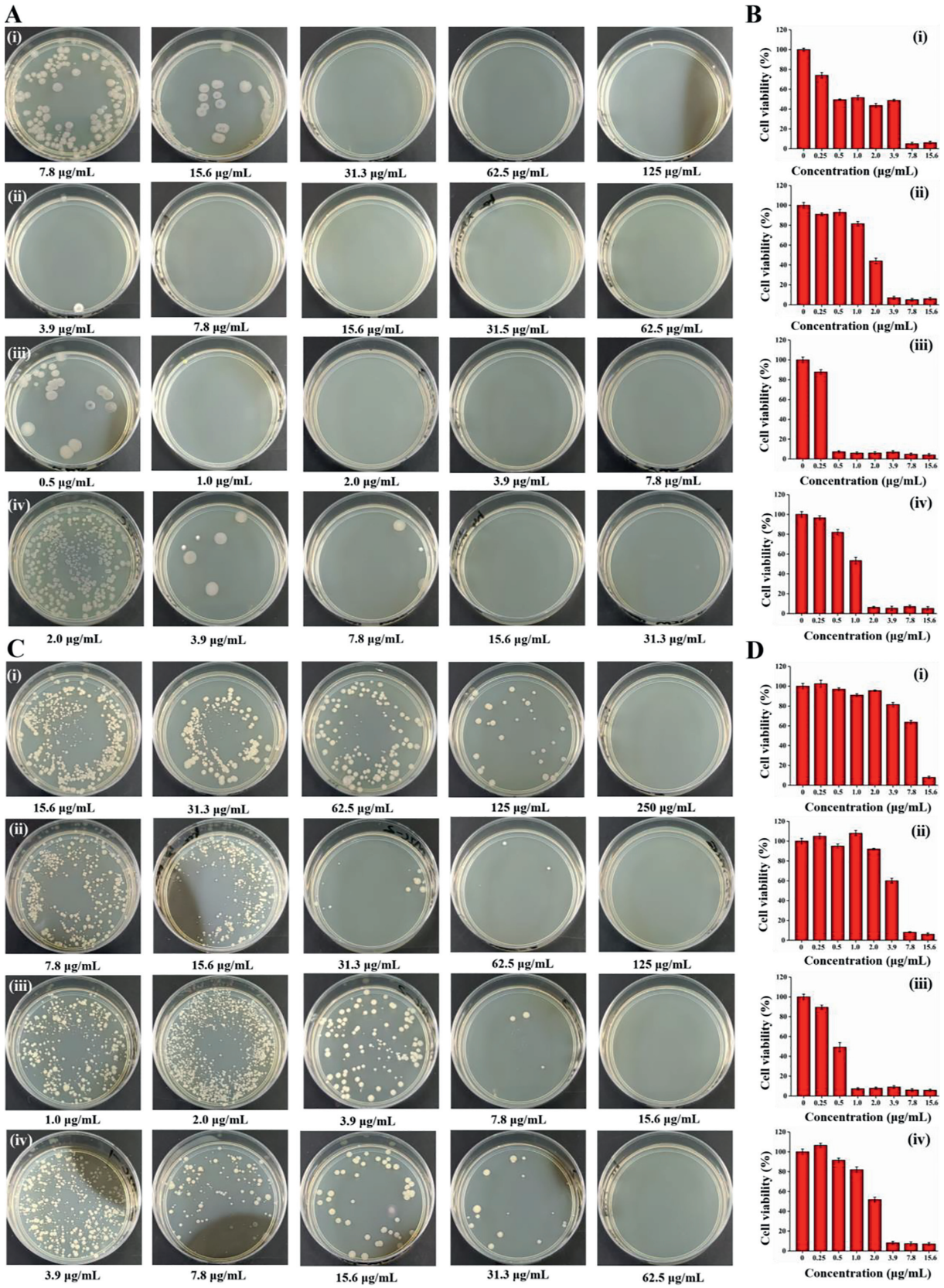

Fig. 3. MBC measurements against (A) *E. coli* and (C) *S. aureus*: (i) T1, (ii) T2, (iii) T3 and (iv) T4. Bacterial cell viability of (B) *E. coli* and (D) *S. aureus*: (i) T1, (ii) T2, (iii) T3 and (iv) T4.

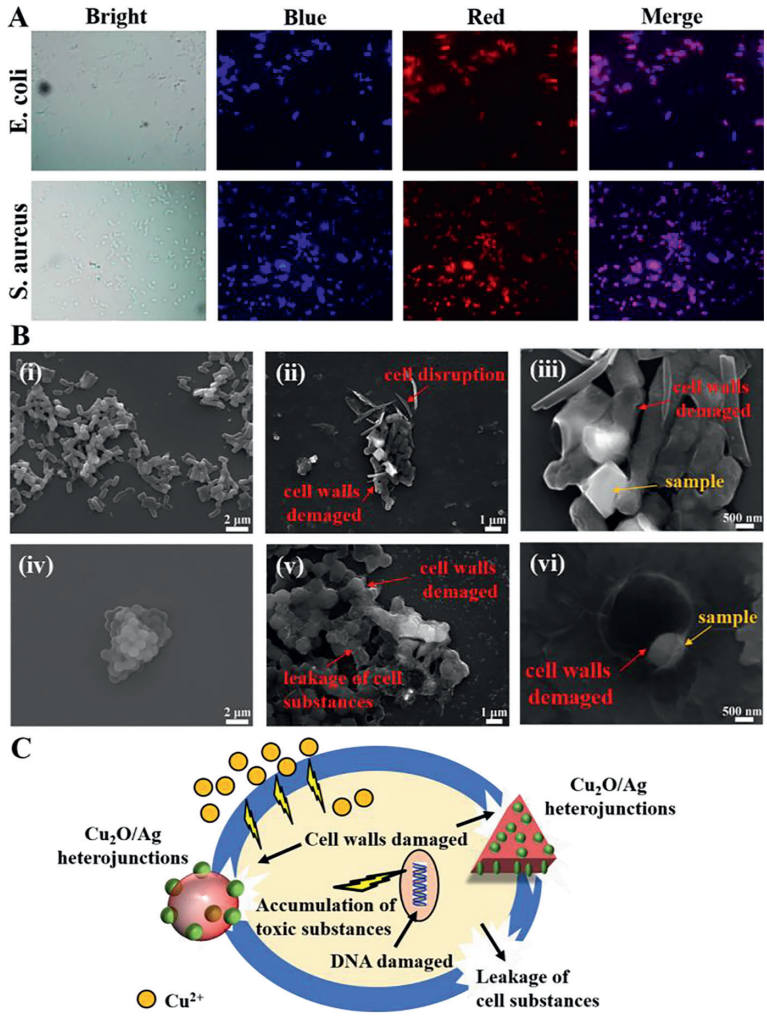

Fig. 4. (A) Fluorescence images of live and dead bacterial cells after incubation with T3 at a concentration of 50 μg/mL for 1 h. (B) Effects of T3 composites on the morphology of *E. coli* and *S. aureus* as examined by scanning electron microscopy: (i) *E. coli* without any treatment, (ii) *E. coli* treated with T3 particles, (iii) the larger multiples of (ii), (iv) *S. aureus* without any treatment, (v) *S. aureus* treated with T3 particles, and (vi) the larger multiples of (v). (C) Schematic illustration of the possible synergistic antibacterial mechanism of Cu_2O/Ag heterojunctions (T3).

brane more easily. To better understand the antimicrobial mechanism, SEM was used to study the interactions between T3 composites and bacteria. As shown in image i in Fig. 4B, the untreated *E. coli* cells are typically rod-shaped having smooth cell surface with intact cell. Yet, when treated with T3 particles, the number of *E. coli* cells significantly reduces and cells are not intact due to the distortion and deformation of cell wall and cell membrane (Fig. 4B, images ii and iii). Significant loss of integrity of cell membrane may possibly lead to the death of cell. Similarly, untreated Gram-positive *S. aureus* cells are generally spherical, having smooth and normal cell wall and cell membrane (Fig. 4B, image iv). After treating with Cu_2O/Ag, *S. aureus* cells are not intact due to the distortion and deformation of cell wall and cell membrane and much substance in the cells leaks out, representing significant loss of integrity of cell membrane that may possibly bring about cell death (Fig. 4B, image v). As shown in image vi in Fig. 4B, Cu_2O/Ag particles are tightly adsorbed by the bacteria surface, leading to the deformation and damage of the cell membrane, which is the reason that the bacteria are eliminated.

According to previous studies, the bactericidal mechanism of Cu_2O is mainly the release of Cu^{2+} ions and the promotion of the production and accumulation of reactive oxygen species (ROS) inside bacteria [28,29]. The bactericidal mechanism of Ag nanoparticles is mainly the puncture effect of the tiny size on bacterial cell membranes [30]. The synergistic effect of Cu_2O and Ag nanoparticles could promote the migration of electrons and holes from the core of Cu_2O to the surface of Ag, resulting in an increase in the production of ROS that will put destructive oxidative stress to bacteria [14]. The synergistic antibacterial effect of Cu_2O and Ag as a heterojunction is testified in this study. As shown in Fig. 4C, possible multi-level synergistic antibacterial mechanisms are proposed: 1) The formation of Cu_2O/Ag heterojunction enhanced the adsorption capacity, and its sharp edges had a significant piercing effect on the bacterial surface, resulting in the bacteria to burst and die; 2) The released Cu^{2+} is quite toxic to bacteria; 3) Cu_2O/Ag could promote surface charge transfer, and the transferred electrons and holes would induce excessive accumulation of toxic substances that damage DNA, inactivate protein and finally kill bacteria.

In summary, Cu_2O/Ag heterojunctions were developed using a green microwave-assisted method in this work. The microwave-assisted synthesis of Cu_2O/Ag heterostructures exhibit much better antibacterial properties than that of pristine Cu_2O. Besides, T3 (n_{AgNO3}:$n_{Cu(Ac)2}$ = 1:9) has a heterogeneous structure of microspheres/triangular sheets that is different from other samples, resulting in better adsorption and sterilization of bacteria. The in-

vestigation of the antibacterial mechanism of Cu_2O/Ag heterojunctions suggests that the mechanical damage to the cell membrane by the sharp edges, the release of Cu^{2+} ions, and the promotion of the rapid production of toxic substances contributed to the antibacterial activity together. Thus, the synergistic effect of Cu_2O/Ag heterojunction makes it a potential candidate that can be exploited for various biomedical and other industrial applications. Additionally, the excellent performance of the microwave-assisted method in the fast, green and efficient synthesis of two-phase heterojunctions provide novel research ideas for the modification of inorganic fungicides.

Declaration of competing interest

There are no conflicts to declare.

Acknowledgments

This work was financially supported by the National Natural Science Foundation of China (Nos. U2004177 and 21504082), Zhongyuan Thousand Talents Plan Project, Outstanding Youth Fund of Henan Province (No. 212300410081) and Natural Science Research Project of Henan Educational Committee (No. 20A43001).

Supplementary materials

Supplementary material associated with this article can be found, in the online version, at doi:10.1016/j.cclet.2021.07.018.

References

[1] X. Liu, J. Iocozzia, Y. Wang, et al., Energ. Environ. Sci. 10 (2017) 402–434.
[2] S. Back, M.H. Hansen, J.A.G. Torres, et al., ACS Appl. Mater. Inter. 11 (2019) 2006–2013.
[3] L. Cai, Y. Du, X. Guan, et al., Chin. Chem. Lett. 30 (2019) 2363–2367.
[4] S. Sun, Nanoscale 7 (2015) 10850–10882.
[5] W. Ahmad, M.M. Hassan, J. Wang, et al., Anal. Methods 11 (2019) 6004–6012.
[6] Z.P. Li, Y.Q. Wen, J.P. Shang, et al., Chin. Chem. Lett. 25 (2014) 287–291.
[7] X. Li, Y. Shang, J. Lin, et al., Adv. Funct. Mater. 28 (2018) 1801868.
[8] B.Le Ouay, F. Stellacci, Nano Today 10 (2015) 339–354.
[9] Y. Qiao, J. He, W. Chen, et al., ACS Nano 14 (2020) 3299–3315.
[10] X. Zhao, Y. Han, T. Zhu, et al., J. Biomed. Nanotechnol. 15 (2019) 1213–1222.
[11] J. Xia, W. Wang, X. Hai, et al., Chin. Chem. Lett. 30 (2019) 421-424.
[12] Y. Liu, D. Li, J. Ding, et al., Chin. Chem. Lett. 31 (2020) 3001–3014.
[13] S. Li, S. Dong, W. Xu, et al., Adv. Sci. 5 (2018) 1700527.
[14] Z. Yang, C. Ma, W. Wang, et al., J. Colloid. Interf. Sci. 557 (2019) 156–167.
[15] G. Meng, X. Wang, H. Hu, et al., Mater. Res. Express. 6 (2019) 105080.
[16] Z. Guo, L. Shi, H. Feng, et al., Chin. Chem. Lett. 32 (2021) 1046–1050.
[17] J. Lin, Y. Shang, X. Li, et al., Adv. Mater. 29 (2017) 1604797.
[18] W. Zhang, X. Yang, Q. Zhu, et al., Ind. Eng. Chem. Res. 53 (2014) 16316–16323.
[19] H. Qin, Q. Wei, J. Wu, et al., Mater. Chem. Phys. 232 (2019) 240–245.
[20] M. Yang, J.J. Zhu, J. Cryst. Growth 256 (2003) 134–138.
[21] B. Fan, Y. Li, F. Han, et al., J. Mater. Sci. Mater. Med. 29 (2018) 69.
[22] W. Duan, M. Zheng, R. Li, et al., J. Nanopart. Res. 18 (2016) 342.
[23] J. Zhou, C. Wang, A.J. Cunningham, et al., Mat. Sci. Eng. C 101 (2019) 499–504.
[24] M.N. Rani, M. Murthy, N.S. Shree, et al., Ceram. Int. 45 (2019) 25020–25026.
[25] G. Applerot, J. Lellouche, A. Lipovsky, et al., Small 8 (2012) 3326–3337.
[26] F. Han, S. Lv, Z. Li, et al., NPG Asia Mater 12 (2020) 1–11.
[24] B. Ramalingam, T. Parandhaman, S.K. Das, ACS Appl. Mater. Inter. 8 (2016) 4963–4976.
[28] S. AlYahya, B.J. Rani, G. Ravi, et al., J. Mater. Sci. Mater. El. 29 (2018) 17622–17629.
[29] J. Li, Z. Li, Z. Liang, et al., Drug Deliv. 25 (2018) 938–949.
[30] M. Akter, M.T. Sikder, M.M. Rahman, et al., J. Adv. Res. 9 (2018) 1–16.